applied sciences

MDPI

Article

Compensation Method for Diurnal Variation in Three-Component Magnetic Survey

Quanming Gao [1], Defu Cheng [1,2], Yi Wang [1], Supeng Li [1], Mingchao Wang [1], Liangguang Yue [1] and Jing Zhao [1,2,*]

1 College of Instrumentation and Electrical Engineering, Jilin University, Changchun 130061, China; gaoqm17@mails.jlu.edu.cn (Q.G.); chengdefu@jlu.edu.cn (D.C.); wangyi@jlu.edu.cn (Y.W.); Lisp@mails.jlu.edu.cn (S.L.); Wangmc18@mails.jlu.edu.cn (M.W.); yuelg18@mails.jlu.edu.cn (L.Y.)

2 Key Laboratory of Geophysical Exploration Equipment (Jilin University), Ministry of Education, Changchun 130061, China

* Correspondence: zhaojing_8239@jlu.edu.cn

Received: 15 January 2020; Accepted: 30 January 2020; Published: 3 February 2020

check for updates

Abstract: Considering that diurnal variation interferes with three-component magnetic surveys, which inevitably affects survey accuracy, exploring an interference compensation method of high-precision is particularly desirable. In this paper, a compensation method for diurnal variation is proposed, the procedure of which involves calibrating the magnetometer error and the misalignment error between magnetometer and non-magnetic theodolite. Meanwhile, the theodolite is used to adjust the attitude of the magnetometer to unify the observed diurnal variation into the geographic coordinate system. Thereafter, the feasibility and validity of the proposed method were verified by field experiments. The experimental results show that the average error of each component between the observed value of the proposed method and that of Changchun Geomagnetic station is less than 1.2 nT, which indicates that the proposed method achieves high observation accuracy. The proposed method can make up for the deficiency that traditional methods cannot meet the requirements of high accuracy diurnal variation compensation. With this method, it is possible for us to set up temporary diurnal variation observation station in areas with complex topography and harsh environment to assist aeromagnetic three-component survey.

Keywords: diurnal variation; three-component magnetic survey; magnetic interference; tri-axial magnetometer; non-magnetic theodolite

1. Introduction

Compared with the scalar magnetic survey, three-component magnetic survey can obtain richer magnetic information, facilitate making quantitative interpretation of magnetic anomaly and enhance the resolution of magnetic target positioning, which plays an important role in geological survey, mineral exploration and earth science research [1–5]. However, the magnetic survey accuracy is inevitably decreased by diurnal variation, thus making it of great importance to develop an effective method for interference compensation.

The magnetic field measured by tri-axial magnetometer can be modeled as the sum of three components

$$\boldsymbol{h}_m = \boldsymbol{h}_g + \boldsymbol{h}_i + \boldsymbol{h}_o$$

Where $\boldsymbol{h}_m$ denotes the measured data, $\boldsymbol{h}_g$ denotes the geomagnetic field, $\boldsymbol{h}_i$ denotes the magnetic interference field, and $\boldsymbol{h}_o$ denotes the diurnal variation interference.

In practice of three-component magnetic survey, the first component is considered as a valuable element while the other two components are as magnetic interference. The magnetic interference field is mainly generated by ferromagnetic material and the maneuvers of carrier [6,7]. Different from the magnetic interference field, diurnal variation represents drift of the geomagnetic field with time. As a matter of fact, diurnal variation can be compensated by simultaneously recording the geomagnetic field variation and then directly subtracting these variation data from the magnetic survey data. Although the established geomagnetic stations can provide accessible diurnal variation information for certain magnetic survey work, the diurnal variation accuracy of magnetic survey area far from the fixed stations will be decreased to a large extent. At present, some researchers have been trying to compensate the diurnal variation by modeling. For instance, Williams [8] regards the diurnal variation as a function of magnetic survey time and compensates it by utilizing a neural network. However, this method can merely estimate the expectation of diurnal variation.

Addressing the deficiencies of the above methods, a novel compensation method is proposed in the paper. Considering that the diurnal variation is the vector data, the prerequisite for compensating diurnal variation is to unify it into a coordinate system with the three-component magnetic survey data. With the proposed method, the diurnal variation is accurately observed in the geographic coordinate system, based on which, the interference can be effectively compensated. In addition, this method enables us to establish movable diurnal observation station in magnetic survey area, thus ensuring the compensation accuracy of diurnal variation to the largest extent. The proposed method is composed of three main procedures: (1) calibrating the magnetometer error; (2) calibrating the misalignment error between the magnetometer and theodolite; (3) aligning the magnetometer's axial direction and true north.

The rest of the paper is organized as follows. Section 2 includes measurement error analysis and introduction on the corresponding calibration method. Section 3 describes the experimental setup and presents the experimental results. Section 4 presents the conclusion.

2. Methods

2.1. Magmetometer Error Calibration

Manufacturing errors inevitably occur in the production of a magnetometer sensor. These errors are generally defined as magnetometer error, existing in the form of scaling error, offset error, and non-orthogonality error [9,10].

1. Scaling error. Scaling error denotes the difference in sensitivity of each axis due to the different characteristics of the internal electronic devices. The scaling error matrix $\boldsymbol{k}_{sf}$ can be modeled as

$$\boldsymbol{k}_{sf} = diag[k_1, k_2, k_3] \tag{1}$$

where k_1, k_2, k_3 denote the axial scaling errors of the magnetometer respectively.

2. Offset error. Offset error denotes the deviation between magnetometer's output and true value, which can be modeled as

$$\boldsymbol{h}_b = [h_b^x, h_b^y, h_b^z]^T \tag{2}$$

where h_b^x, h_b^y, h_b^z denote the axial offset errors of the magnetometer respectively.

3. Non-orthogonality error. The orthogonality between three axes of the magnetometer cannot be guaranteed due to manufacturing precision limitations, thus resulting in non-orthogonal error, as illustrated in Figure 1. As is shown, $o - xyz$ denotes the ideal tri-axial magnetometer while $o' - x'y'z'$ denotes the non-orthogonal magnetometer.

The non-orthogonality error matrix $\boldsymbol{k}_{nor}$ can be modeled as

$$\boldsymbol{k}_{nor} = \begin{bmatrix} cos\varphi cos\phi & cos\varphi sin\phi & sin\varphi \\ 0 & cos\psi & sin\psi \\ 0 & 0 & 1 \end{bmatrix} \tag{3}$$

where ϕ, φ, ψ denote the error angles.

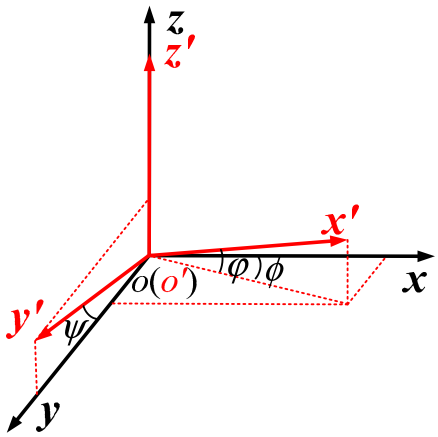

Figure 1. Diagram of the non-orthogonality error.

The comprehensive mathematical model for output error of the magnetometer interfered by different error sources can be expressed as

$$\boldsymbol{h}_m = \boldsymbol{k}_{sf}\boldsymbol{k}_{nor}\boldsymbol{h}_g + \boldsymbol{h}_b \tag{4}$$

where $\boldsymbol{h}_m$ denotes the measured data of the magnetometer, $\boldsymbol{h}_g$ denotes the true geomagnetic field.

According to Equation (4), the calibration model of magnetometer error can be expressed as

$$\boldsymbol{h}_g = \boldsymbol{k}(\boldsymbol{h}_m - \boldsymbol{h}_b) \tag{5}$$

where $\boldsymbol{k} = \boldsymbol{k}_{nor}^{-1}\boldsymbol{k}_{sf}^{-1}$.

We can get

$$\|\boldsymbol{h}_g\|^2 = \boldsymbol{h}_g^T\boldsymbol{h}_g = (\boldsymbol{h}_m - \boldsymbol{h}_b)^T\boldsymbol{k}^T\boldsymbol{k}(\boldsymbol{h}_m - \boldsymbol{h}_b) \tag{6}$$

then

$$\frac{(\boldsymbol{h}_m - \boldsymbol{h}_b)^T\boldsymbol{k}^T\boldsymbol{k}(\boldsymbol{h}_m - \boldsymbol{h}_b)}{\|\boldsymbol{h}_g\|^2} = 1 \tag{7}$$

In areas with stable magnetic field, the magnitude of the geomagnetic field remains constant within a short period, so as the magnetometer rotates, its measuring locus will form a sphere with a radius equal to the magnitude of the local geomagnetic field [11]. However, due to the magnetometer error, the sphere is distorted into an ellipsoid [12].

The equation of quadric surface is

$$F(\rho, \sigma) = \rho^T\sigma = ax^2 + by^2 + cz^2 + 2dxy + 2exz + 2fyz + 2px + 2qy + 2rz + g = 0 \tag{8}$$

where $\rho = [a, b, c, d, e, f, p, q, r, g]^T$, $\sigma = [x^2, y^2, z^2, 2xy, 2xz, 2yz, 2x, 2y, 2z, 1]^T$.

Let $v = [H_m^x{}^2, H_m^y{}^2, H_m^z{}^2, 2H_m^xH_m^y, 2H_m^xH_m^z, 2H_m^yH_m^z, 2H_m^x, 2H_m^y, 2H_m^z, 1]^T$, $F(\rho, v)$ denotes the distance from the measuring point $\boldsymbol{h}_m = \left[h_m^x, h_m^y, h_m^z\right]^T$ to the quadric surface $F(\rho, \sigma) = 0$. Therefore, the parameter ρ can be solved by fitting based on the minimum value of $F(\rho, v)$. That is,

$$\sum_{i=1}^{n} \|F(\rho, v_i)\|^2 = min \tag{9}$$

The quadric surface has multiple forms such as ellipsoid, cylinder, parabola, etc. In the mathematical sense, to ensure that the fitted quadric surface is an ellipsoid, it is required to add the following constraints in the fitting process.

$$I_1 \neq 0, \quad I_2 > 0, \quad I_1 \cdot I_3 > 0, \quad I_4 < 0$$

where $I_1 = a + b + c$, $\quad I_2 = \begin{vmatrix} b & f \\ f & c \end{vmatrix} + \begin{vmatrix} c & e \\ e & a \end{vmatrix} + \begin{vmatrix} a & d \\ d & b \end{vmatrix}$, $\quad I_3 = \begin{vmatrix} a & d & e \\ d & b & f \\ e & f & c \end{vmatrix}$, $\quad I_4 = \begin{vmatrix} a & d & e & p \\ d & b & f & q \\ e & f & c & r \\ p & q & r & g \end{vmatrix}$.

After obtaining the parameter ρ, the Equation $F(\rho, v) = 0$ can be written as the following matrix form

$$\boldsymbol{h}_m^T \boldsymbol{E} \boldsymbol{h}_m + 2\boldsymbol{F}\boldsymbol{h}_m + g = 0 \tag{10}$$

where $\boldsymbol{E} = \begin{bmatrix} a & d & e \\ d & b & f \\ e & f & c \end{bmatrix}$, $\boldsymbol{F} = \begin{bmatrix} p \\ q \\ r \end{bmatrix}$.

Then, convert Equation (10)

$$(\boldsymbol{h}_m - \boldsymbol{X}_0)^T \boldsymbol{A}_e (\boldsymbol{h}_m - \boldsymbol{X}_0) = 1 \tag{11}$$

where $\boldsymbol{X}_0 = -\boldsymbol{E}^{-1}\boldsymbol{F}$, $\quad \boldsymbol{A}_e = \frac{\boldsymbol{E}}{\boldsymbol{F}^T\boldsymbol{E}^{-1}\boldsymbol{F} - g}$.

Comparing Equation (7) and Equation (11), we can get

$$\begin{cases} \boldsymbol{h}_b = \boldsymbol{X}_0 \\ \frac{\boldsymbol{k}^T\boldsymbol{k}}{||\boldsymbol{h}_g||^2} = \boldsymbol{A}_e \end{cases} \tag{12}$$

Here, as $\boldsymbol{A}_e$ is a positive definite matrix, Cholesky decomposition can be applied

$$\boldsymbol{A}_e = \boldsymbol{R}^T\boldsymbol{R} \tag{13}$$

Then, we can get

$$\boldsymbol{k} = \sqrt{||\boldsymbol{h}_g||^2}\boldsymbol{R} \tag{14}$$

2.2. Misalignment Error Calibration

In this method, a high accuracy non-magnetic theodolite is used to precisely adjust the attitude of the magnetometer, so as to unify the observed diurnal variation into the geographic coordinate system. For this purpose, we need to calibrate misalignment error between the magnetometer and the theodolite. Figure 2 illustrates misalignment error between the magnetometer and the theodolite. As is shown, we define two coordinate systems: the magnetometer coordinate system ($o_m - x_m y_m z_m$) and the theodolite coordinate system ($o_t - x_t y_t z_t$), in which x_m, y_m, z_m and x_t, y_t, z_t denote three axes of the magnetometer and the theodolite respectively.

According to the Euler-angle rotation method [13], three rotations can re-orient an object in any direction. This method can be applied to calibrate the misalignment error. Here,

$$\text{rotation matrix} = \begin{bmatrix} \text{rotated } y_m - \text{axis} \\ \text{rotated } x_m - \text{axis} \\ \text{rotated } z_m - \text{axis} \end{bmatrix} \tag{15}$$

The process can be described by the following rotation matrices.

$$C_{x_m-axis} = \begin{bmatrix} 1 & 0 & 0 \\ 0 & \cos\beta & -\sin\beta \\ 0 & \sin\beta & \cos\beta \end{bmatrix} \quad (16)$$

$$C_{y_m-axis} = \begin{bmatrix} \cos\gamma & 0 & \sin\gamma \\ 0 & 1 & 0 \\ -\sin\gamma & 0 & \cos\gamma \end{bmatrix} \quad (17)$$

$$C_{z_m-axis} = \begin{bmatrix} \cos\alpha & -\sin\alpha & 0 \\ \sin\alpha & \cos\alpha & 0 \\ 0 & 0 & 1 \end{bmatrix} \quad (18)$$

where α, β, γ denote the misalignment error angles.

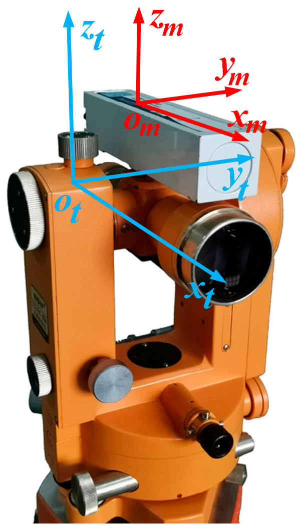

Figure 2. Diagram of misalignment error between the non-magnetic theodolite and the magnetometer.

The final rotation matrix C_m^t can be found by multiplying these together.

$$C_m^t = C_{z_m-axis} C_{x_m-axis} C_{y_m-axis} \quad (19)$$

With the known error angles, the transformation of measured data from the magnetometer coordinate system to the theodolite coordinate system is given by

$$\begin{bmatrix} x_t \\ y_t \\ z_t \end{bmatrix} = C_m^t \begin{bmatrix} x_m & y_m & z_m \end{bmatrix}^T \quad (20)$$

In this paper, we adopted an approach to identify the three misalignment error angles by rotation. When rotating the magnetometer around one axis of the theodolite, the projection of geomagnetic field on the axis of the magnetometer aligned with the rotation axis is constant after calibrating misalignment error, which serves as the basis for calibration method.

According to Equation (20), the measured data are substituted into the following equation to calibrate the misalignment error.

$$\boldsymbol{h} = C_m^t \boldsymbol{h}_m \quad (21)$$

where $\boldsymbol{h}_m$ denotes the measured data of the magnetometer rotating around one axis of the theodolite.

Let

$$\boldsymbol{v} = \begin{bmatrix} v_x \\ v_y \\ v_z \end{bmatrix} = \boldsymbol{h}(i) - \boldsymbol{h}(j) \quad (i \neq j) \tag{22}$$

As analyzed above, v_x is constant during the rotation around x_t-axis. Similarly, v_y and v_z remain unchanged as well when rotating around y_t-axis and z_t-axis respectively. Thus, we can get

$$v_c(i) - v_c(j) = 0 \quad c \in \{x, y, z\} \tag{23}$$

The objective function is defined as

$$l(\alpha, \beta, \gamma) = \min_{c \in \{x,y,z\}} \sum_{i=1}^{n-1} \sum_{j=i+1}^{n} \left| v_c(i) - v_c(j) \right| \tag{24}$$

This optimization design aims to estimate three misalignment error angles by minimizing the objective function. The optimization process solves this nonlinear system with multiple objectives using the least square method [14].

Rotating the magnetometer around one axis of the theodolite can only align this axis to the magnetometer's axis of the same direction, which means rotating the magnetometer around y_t-axis of the theodolite only ensures the alignment of y_t-axis to y_m-axis. Therefore, it is required to rotate the magnetometer around at least two axes of the theodolite respectively so as to calibrate the misalignment error. Meanwhile, it should be noted that rotation in pitch (rotating around y_t-axis) of the magnetometer ought to be avoided after calibrating the misalignment error, otherwise it will invalidate the obtained misalignment error angles (α, β, γ).

2.3. Alignment to North

The geographic coordinate system with three axes pointing to north, east and up respectively is taken as the datum coordinate system for magnetic survey. Here, the north direction is the geographic North Pole, also known as true north. After finishing the above two steps of calibration, we will discuss how to align the axis of magnetometer to true north in this part.

As illustrated in Figure 3, θ is the angle between the line of two sites (A and B) of distance d and true north direction. The challenge of aligning to true north direction is to obtain the angle θ accurately. Here, the angle θ can be calculated by the following steps. Firstly, the latitude and longitude of the selected sites A and site B are measured using differential GPS. Then, the latitude L and longitude B are converted into x and y coordinate values of plane coordinates by means of coordinate transformation to obtain the relative position of sites A and B [15]. The transformation of the coordinate system is as follows.

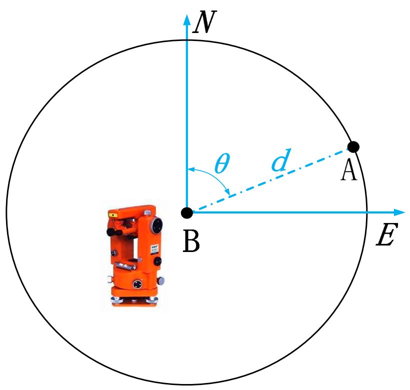

Figure 3. Diagram of aligning to north.

The arc length $\tau(B)$ of an ellipsoid from the equator to the site is given by

$$\tau(B) = \alpha(B + \beta \sin 2B + \gamma \sin 4B + \delta \sin 6B + \varepsilon \sin 8B) \quad (25)$$

where

$$\begin{aligned}
\alpha &= \tfrac{a+b}{2}\left(1 + \tfrac{1}{4}n^2 + \tfrac{1}{64}n^4\right) \\
\beta &= -\tfrac{3}{2}n + \tfrac{9}{16}n^3 - \tfrac{3}{32}n^5 \\
\gamma &= \tfrac{15}{16}n^2 - \tfrac{15}{32}n^4 \\
\delta &= -\tfrac{35}{48}n^3 + \tfrac{105}{256}n^5 \\
\varepsilon &= \tfrac{315}{512}n^4 \\
n &= \tfrac{a-b}{a+b} \\
b &= a\left(1 - \tfrac{1}{F}\right)
\end{aligned}$$

with 'a' denoting the semi-major axis of the earth, 'F' denoting the flattening factor of the earth.

The prime vertical radius of curvature N is

$$N = \frac{a}{\sqrt{1 - e^2 \sin^2 B}} \quad (26)$$

where the first eccentricity of earth e is

$$e = \frac{\sqrt{a^2 - b^2}}{a} \quad (27)$$

The transformation equation is given by

$$\begin{aligned}
x = \tau(B) &+ \tfrac{t}{2}N\cos^2 B(L - L_0)^2 + \tfrac{t}{24}N\cos^4 B\left(5 - t^2 + 9\eta^2 + 4\eta^4\right)(L - L_0)^4 \\
&+ \tfrac{t}{720}N\cos^6 B\left(61 - 58t^2 + t^4 + 270\eta^2 - 330t^2\eta^2\right)(L - L_0)^6 \\
&+ \tfrac{t}{40320}N\cos^8 B\left(1385 - 3111t^2 + 543t^4 - t^6\right)(L - L_0)^8
\end{aligned} \quad (28)$$

$$\begin{aligned}
y = y_o &+ N\cos B(L - L_0) + \tfrac{1}{6}N\cos^3 B\left(1 - t^2 + \eta^2\right)(L - L_0)^3 \\
&+ \tfrac{1}{120}N\cos^5 B\left(5 - 18t^2 + t^4 + 14\eta^2 - 58t^2\eta^2\right)(L - L_0)^5 \\
&+ \tfrac{1}{5040}N\cos^7 B\left(61 - 478t^2 + 179t^4 - t^6\right)(L - L_0)^7
\end{aligned} \quad (29)$$

with 'L_0' denoting the longitude of central meridian. Where $t = \tan B$, $\eta = \frac{e^2}{1-e^2}$, y_o =500,000.

We can substitute the coordinate values of sites A and B into Equation (30) to calculate the angle θ. Theoretically, the farther the distance between sites A and B, the higher the accuracy of angle θ is. A distance between the two sites no less than 100 m is acceptable.

$$\theta = \arctan\left|\frac{y_A - y_B}{x_A - x_B}\right| \quad (30)$$

where (x_A, y_A) and (x_B, y_B) are coordinate values of the sites A and B respectively.

Before aligning the axis of magnetometer to true north direction using the obtained angle θ, the following preparations are quite necessary: (1) place the theodolite on the site B using the optical plummet; (2) level the theodolite by adjusting the leveling foot screw; (3) align the reticle of objective lens to site A by adjusting the theodolite. After making the above preparations, the coming procedure is to rotate the theodolite to align the axis of magnetometer to true north. It should be noted that the relative position of sites A and B will affect the rotation angle of the theodolite. There are four different situations for the relative position of sites A and B, which can be expressed in quadrants as: NE-quadrant, NW-quadrant, SW-quadrant, and SE-quadrant, as illustrated in Figure 4. The rotation angle $= \theta_i$ $(i = 1, 2)$ when the relative position is in NE-quadrant and NW-quadrant while rotation angle $= 180^0 - \theta_i$ $(i = 3, 4)$ in SW-quadrant and SE-quadrant.

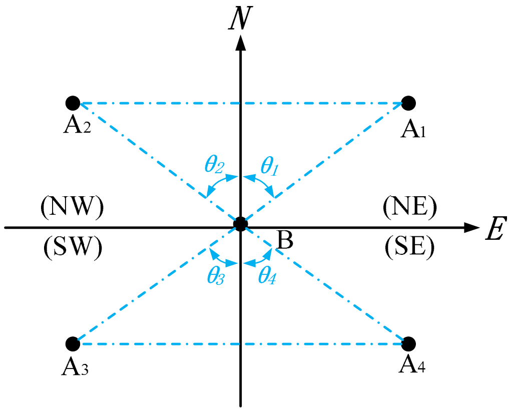

Figure 4. Relative position of site A and B.

3. Experiments

3.1. Experimental Setup

In order to verify the feasibility and validity of the proposed method, a diurnal variation observation system consisting of a tri-axial magnetometer (MAG-03MS100, Bartington, Witney, Britain), a non-magnetic theodolite (TDJ2E-NM, Boif, Beijing, China) and a differential GPS (IMU-IGM-S1, Novatel, Calgary, AB, Canada) was built in the experiment. The performance specifications of the experimental setup are shown in Table 1.

Table 1. Performance specifications of experimental devices

Device	Quantity	Value
Magnetometer	Measuring range	±100 uT
	Measurement noise floor	6~10 pT/√Hz at 1 Hz
	Non-orthogonality error	<0.1°
	Scaling error	<±0.5%
	Offset error	≤±5 nT
Non-magnetic theodolite	Magnetic contamination	≤1 nT
	Plate level	20″/2 mm
	Mean squared error of a horizontal measured face left/right	2″
	Mean squared error of a vertical measured face up/down	6″
	Initial horizontal misalignment	<20″
	Initial vertical misalignment	<25″
Differential GPS	Position accuracy (RMS)	horizontal 0.02 m
		vertical 0.03 m

As described previously, the magnetometer error, misalignment error, and alignment to the north are calibrated successively. The relevant experiment was carried out in an area within 100 m far from Changchun Geomagnetic station. There is no magnetic interference around the selected area. In addition, the six-channel spectrum analyzer Spectramag-6 supporting the use of Mag-03MS100 magnetometer is adopted as the data acquisition unit.

3.2. Calibration Results

The total field intensity of experimental site measured by GSM-19 Overhauser magnetometer (GEM Systems, Markham, ON, Canada) is 55,046.65 nT, which is used as a reference for calibrating the magnetometer error. During the process of data collection, the magnetometer is rotated to capture samples with different attitudes. From Figure 5a, it can be seen that interfered by the magnetometer error, the measurement locus appears as an ellipsoid. With the fitted ellipsoid, we are capable of obtaining the magnetometer error calibration parameters $\boldsymbol{k}$ and $\boldsymbol{h}_b$. Figure 5b illustrates the calibration result, from which we can see that the maximum residual of total field is reduced from 105 nT to less than 3 nT, indicating a significant decrease in the measurement error of the magnetometer.

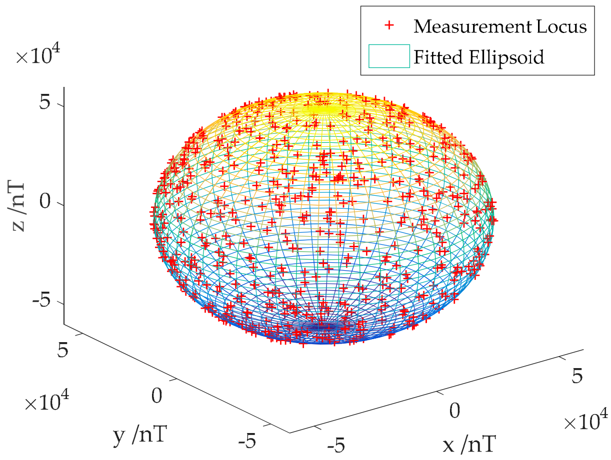

(a)

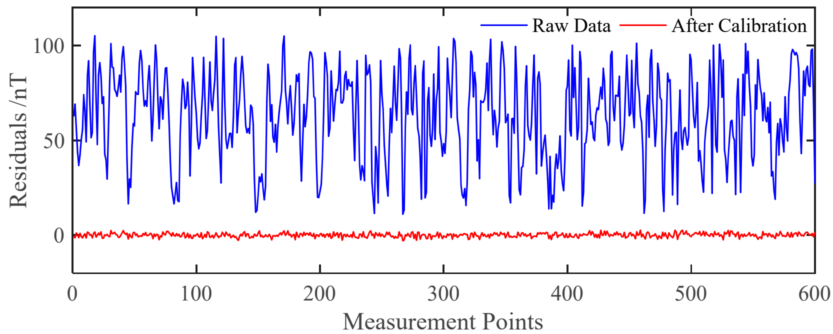

(b)

Figure 5. Calibration result of magnetometer error: (**a**) The measurement locus and the fitted ellipsoid; (**b**) The residual of total field after calibration.

In the misalignment error calibration experiment, rotations of the magnetometer around y_t-axis and z_t-axis are performed separately to obtain experimental data. As mentioned above, the pitch angle of the magnetometer ought to avoid being changed after calibrating misalignment error. Hence, the rotation sequence is first around y_t-axis and then z_t-axis. Figure 6 illustrates the misalignment error calibration result. It can be seen that, interfered by the misalignment error during rotation, the fluctuation of y-component exceeds 981.1 nT while that of z-component exceeds 269.2 nT. Meanwhile, we can see that the fluctuations have been reduced to less than 7.4 nT and 5.9 nT respectively after calibration, which indicates the misalignment error is decreased to an acceptable range.

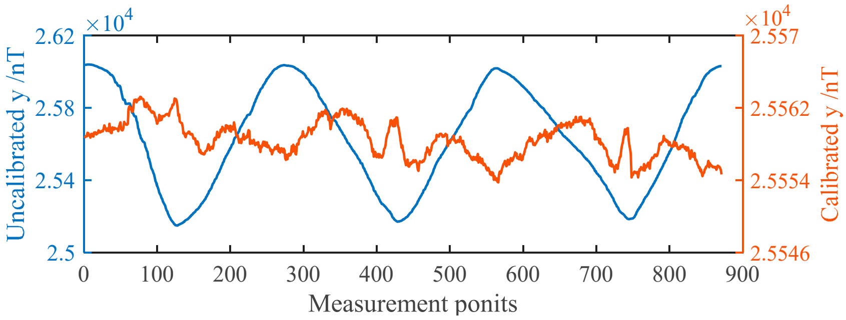

(**a**)

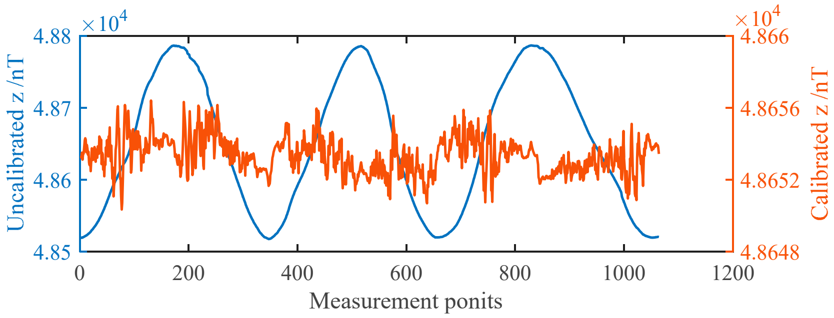

(**b**)

Figure 6. Calibration result of misalignment error: (**a**) calibration result by rotating around y_t-axis; (**b**) calibration result by rotating around z_t -axis.

Prior to aligning the axis of the magnetometer to the true north direction, the theodolite is required to be leveled. With the help of a high-precision plate level, the horizontal error can be restricted within 20″ after leveling. In the procedure of aligning to the north, the latitude and longitude of the selected sites A and B are measured as (44.08735182° N, 124.90305218° E) and (44.0875215302° N, 124.90305218° E), as illustrated in Figure 7. The angle θ is calculated to be 83.49442° using the above positional parameters. Meanwhile, the relative position of the two sites is in SW-quadrant, which means the theodolite requires to be rotated 96.50558° in the north direction to align the x_t-axis of magnetometer to the true north.

Figure 7. Diurnal variation observation system.

After the above steps of calibration, it can be assumed that the magnetometer error and misalignment error have been eliminated and the x_t-axis of the magnetometer is aligned to the true north direction.

3.3. Diurnal Variation Observation

In order to evaluate the performance of the proposed method, a field experiment is conducted subsequently. The diurnal variation of 24 h was observed with a sampling frequency of 1 Hz in the experiment. Meanwhile, the diurnal variation obtained by the Changchun Geomagnetic station was used as the reference for evaluating the observation accuracy of the proposed method. Figure 8 illustrates the diurnal variation observations. It can be intuitively seen that the trend of observations of the proposed method is highly consistent with the reference. Besides, two indexes of Pearson correlation coefficient p [16] and average error $\bar{e}$ (Equation (28)) are introduced in the paper to evaluate the performance of the proposed method more objectively, as it is shown in Table 2. The larger p is, the higher the correlation is and the smaller $\bar{e}$ is, the higher the accuracy of observation is. Commonly, $0.8 \le p < 1$ denotes high correlation. The fact that p of each component is greater than 0.8 and $\bar{e}$ is less than 1.2 nT indicates high observation accuracy of the proposed method.

$$p = \frac{\sum_{i=1}^{n}(o(i)-\bar{o})(r(i)-\bar{r})}{\sqrt{\sum_{i=1}^{n}(o(i)-\bar{o})^2}\sqrt{\sum_{i=1}^{n}(r(i)-\bar{r})^2}}$$

$$\bar{e} = \frac{1}{n}\sum_{i=1}^{n}\left|o(i)-r(i)\right| \tag{31}$$

where o denotes observed value and $\bar{o}$ denotes the average value of o, r denotes reference value and $\bar{r}$ denotes the average value of r.

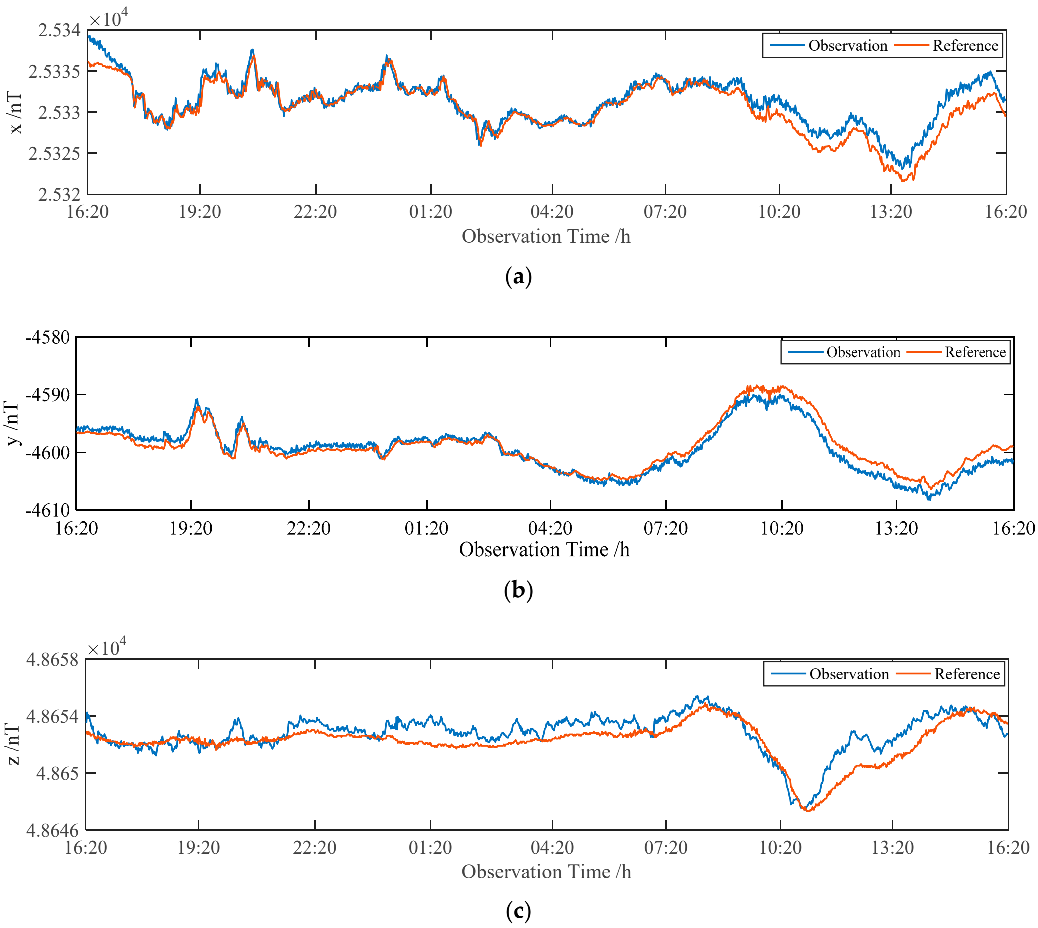

Figure 8. Diurnal variation observations. (**a**) The observed value of x-component; (**b**) The observed value of y -component; (**c**) The observed value of z -component.

Table 2. Evaluation index.

Component	x	y	z
p	0.947	0.951	0.860
$\bar{e}$ (nT)	0.903	1.104	0.726

4. Conclusions

Aiming at the reduction of the diurnal variation in three-component magnetic survey, a compensation method is proposed in the paper. With this method, the diurnal variation in the geographic coordinate system is accurately observed, based on which, the interference can be effectively compensated using the obtained magnetic variation data. The feasibility and validity of the method are verified by field experiment, the results of which indicate that the proposed method can meet the requirement of three-component magnetic survey for diurnal variation compensation accuracy. Compared with the traditional methods, the proposed method overcomes the deficiency of immovability of fixed geomagnetic stations and low compensation accuracy of modeling approach. With the advantages of simple operation and portability of equipment used, the proposed method can be used to assist aeromagnetic three-component survey in areas with special environment such as deserts and forests by setting up the temporary observation station.

Author Contributions: Q.G. proposed the research ideas; Q.G., M.W., and L.Y. conceived the experiments; Q.G., Y.W., and S.L. conducted the experiments; D.C. and J.Z. analyzed the results. All authors reviewed the manuscript. All authors have read and agreed to the published version of the manuscript.

Funding: This work was funded in part by the National Natural Science Foundation of China under Grant 41704172, in part by the National Key Research and Development Project Grant 2016YFC0303000, in part by the National Key Research and Development Project Grant 2017YFC0602000, and Science and Technology Development Plan Project of Jilin Province Grant 20170101065JC.

Acknowledgments: The authors would like to show sincere gratitude to Changchun Geomagnetic station for providing data supports for this work.

Conflicts of Interest: The authors declare no conflict of interest.

References

1. Sheinker, A.; Frumkis, L.; Ginzburg, B.; Salomonski, N.; Kaplan, B.Z. Magnetic anomaly detection using a three-axis magnetometer. *IEEE Trans. Magn.* **2009**, *45*, 160–167. [CrossRef]
2. Tominaga, M.; Tivey, M.A.; MacLeod, C.J.; Morris, A.; Lissenberg, C.J.; Shillington, D.J.; Ferrini, V. Characterization of the in situ magnetic architecture of oceanic crust (Hess Deep) using near-source vector magnetic data. *Geophys. Res.-Solid Earth.* **2016**, *6*, 4130–4146. [CrossRef]
3. Liu, S.; Hu, X.; Cai, J.; Li, J.; Shan, C.; Wei, W.; Liu, Y. Inversion of borehole magnetic data for prospecting deep-buried minerals in areas with near-surface magnetic distortions: A case study from the Daye iron-ore deposit in Hubei, central China. *Near Surf. Geophys.* **2017**, *3*, 298–310. [CrossRef]
4. Munschy, M.; Simon, F. Scalar vector, tensor magnetic anomalies: Measurement or computation? *Geophys. Prospect.* **2011**, *6*, 1035–1045. [CrossRef]
5. Munschy, M.; Boulanger, D.; Ulrich, P.; Bouiflane, M. Magnetic mapping for the detection and characterization of UXO: Use of multi-sensor fluxgate 3-axis magnetometers and methods of interpretation. *J. Appl. Geophys.* **2007**, *3*, 168–183. [CrossRef]
6. Wu, P.; Zhang, Q.; Chen, L.; Fang, G. Analysis on systematic errors of aeromagnetic compensation caused by measurement uncertainties of three-axis magnetometers. *IEEE Sens. J.* **2018**, *1*, 361–369. [CrossRef]
7. Zhang, Q.; Pang, H.F.; Wan, C.B. Magnetic interference compensation method for geomagnetic field vector measurement. *Measurement* **2016**, *91*, 628–633. [CrossRef]
8. Williams, P.M. Aeromagnetic compensation using neural networks. *Neural Comput. Appl.* **1993**, *1*, 207–214. [CrossRef]
9. Jung, J.; Park, J.; Choi, J.; Choi, H.T. Autonomous mapping of underwater magnetic fields using a surface vehicle. *IEEE Access* **2018**, *6*, 62552–62563. [CrossRef]

10. Ousaloo, H.S.; Sharifi, G.H.; Mahdian, J.; Nodeh, M.T. Complete calibration of three-axis strapdown magnetometer in mounting frame. *IEEE Sens. J.* **2017**, *23*, 7886–7893. [CrossRef]
11. Long, D.; Zhang, X.; Wei, X.; Luo, Z.; Cao, J. A fast calibration and compensation method for magnetometers in strap-down spinning projectiles. *Sensors* **2018**, *12*, 4157. [CrossRef] [PubMed]
12. Gebre-Egziabher, D.; Elkaim, G.H.; Powell, J.D.; Parkinson, B.W. Calibration of strapdown magnetometers in magnetic field domain. *J. Aerosp. Eng.* **2006**, *2*, 87–102. [CrossRef]
13. Milligan, T. More applications of Euler rotation angles. *IEEE Antennas Propag. Mag.* **1999**, *4*, 78–83. [CrossRef]
14. Hutcheson, G.D. Ordinary least-squares regression. In *The Multivariate Social Scientist*; SAGE Publications Ltd.: Southend Oaks, CA, USA, 2011; pp. 224–228.
15. Ayer, J.; Fosu, C. Map Coordinate Referencing and the use of GPS datasets in Ghana. *J. Sci. Technol.* **2008**, *1*, 1106–1127. [CrossRef]
16. Zhu, H.; You, X.; Liu, S. Multiple Ant Colony Optimization Based on Pearson Correlation Coefficient. *IEEE Access* **2019**, *7*, 61628–61638. [CrossRef]

© 2020 by the authors. Licensee MDPI, Basel, Switzerland. This article is an open access article distributed under the terms and conditions of the Creative Commons Attribution (CC BY) license (http://creativecommons.org/licenses/by/4.0/).